ELSEVIER

Automation in Construction 13 (2004) 393–407

AUTOMATION IN CONSTRUCTION

www.elsevier.com/locate/autcon

Self-contained automated construction deposition system

Robert L. Williams II[a,*], James S. Albus[b], Roger V. Bostelman[b]

[a] *Department of Mechanical Engineering, Ohio University, 257 Stocker Center, Athens, OH 45701-2979, USA*
[b] *National Institute of Standards and Technology, Gaithersburg, MD, USA*

Abstract

This article presents a novel autonomous system concept for automated construction of houses and other buildings via deposition of concrete and similar materials. The overall system consists of a novel cable-suspended mobility subsystem (a self-contained extension of the RoboCrane), a deposition nozzle subsystem, a metrology subsystem, and a material supply subsystem. This article focuses mainly on the kinematics and statics analysis for control of the self-contained cable-suspended mobility subsystem. We also present alternate design concepts for the mobility system. The purpose of the Cartesian metrology system is to provide an outer-loop controller to provide the required Cartesian pose motions despite uncertainties and unmodeled effects such as cable stretch, wear, and flexibility, plus wind loads.

Keywords: Automated construction; Deposition; Mobility; Metrology; RoboCrane; Cable-suspended; Self-contained; Forward pose kinematics

1. Introduction

Conventional construction cranes that can be seen at any construction site have the following characteristics: nonrigid support; low payload-to-weight ratio (including counterweight); low resistance to wind; inaccurate control of loads; only used to lift and coarsely position loads; limited remote, autonomous capabilities; workers are in a hazardous area; and at any given location, only 1 degree of freedom (*df*) is controlled by the crane (i.e., the length of the lift cable between the boom and object); human workers are required with tag lines to maintain the load's remaining 5 degrees of freedom. This is inefficient, humans have limited strength, and it is dangerous.

To improve upon these undesirable characteristics, the RoboCrane was developed at National Institute of Standards and Technology (NIST) [1,2,6]. The RoboCrane is an inverted Stewart Platform wherein a moving platform is controlled in 6 degrees of freedom via six active cables and winches. Not only can RoboCrane provide lift, but also the remaining 5 degrees of freedom are actively controlled to be stiff and stable (over a limited range of motion and orientations). This concept was extended for a stiff, stable underwater work platform, wherein the platform may be controlled to be stationary even if surrounding seas are not [4].

Inspired by the NIST RoboCrane, many researchers have been involved with cable-suspended robots. A few of these have focused on cable-suspended

* Corresponding author. Tel.: +1-740-593-1096; fax: +1-740-593-0476.
E-mail address: williar4@ohio.edu (R.L. Williams).
URL: http://www.ent.ohiou.edu/~bobw.

0926-5805/$ - see front matter © 2004 Elsevier B.V. All rights reserved.
doi:10.1016/j.autcon.2004.01.001

crane devices. Aria et al. [3] developed a 7 degrees of freedom, three-cable suspended crane-type robot (the remaining freedoms are an *XY* overhead gantry, plus top and bottom turntables) for an automobile assembly line, intended for heavy products assembly. Mikulas and Yang [8] present a three-cable crane design for a lunar construction application, off-loading massive modules from a landing site, moving them, and constructing them into an operational base. Viscomi et al. [11] developed construction automation technology wherein Stewart platform cranes (i.e., RoboCranes) are central. Shanmugasundram and Moon [9] present a dynamic model of a parallel link crane with positioning and orientation capabilities, with unilateral cable constraints. Yamamoto et al. [14] propose a crane-type parallel mechanism with three active cables for handling heavy objects. Shiang et al. [10] present a parallel four-cable positioning crane for offshore loading and unloading of cargo vessels under high sea states. A novel process for deposition of material in construction applications is under development by Khoshnevis [7]. Williams et al. [13] present dynamics modeling and control for cable-based robots, ensuring only positive tensions during all motion.

The RoboCrane has great potential as an automated construction robot system; however, its major drawback is that it requires rigid overhead cable support points which may not exist at most construction sites. Therefore, this article introduces an economical, self-contained, movable-base construction crane for teleoperated and/or autonomous construction applications. Compared to existing commercial and proposed construction cranes, the system is novel because it combines conventional rigid crane members with RoboCrane-type cable suspension and actuation concepts to provide a rigid, lightweight, long-reach, overhead platform. This new concept has the potential to address the shortcomings listed above for conventional crane systems. Furthermore, the self-contained design provides the required rigid overhead cable connection points. This article first presents the overall system concepts, and then mainly focuses on the kinematics equations for control of the self-contained mobility subsystem. We also consider quasi-statics analysis to avoid configurations requiring negative actuating cable tensions. Alternate design concepts are also presented. Lastly, we discuss the proposed controller to ensure sufficient accuracy despite real-world issues such as cable flexibility and wind forces.

2. Overall system description and application

An Automated Construction System concept is under development at NIST, based on self-contained extension of the RoboCrane. The overall system concept, shown constructing a building in Fig. 1, includes 4 major components (see Fig. 2): mobility system (self-contained cable-suspended crane), material deposition system (slip-form tool), metrology system, and material supply system. The overall concept of automated construction of buildings using free-form fabrication is novel and integrates these 4 systems into an advanced construction system capable of manually or autonomously fabricating walls and structures while under manual or computer control, respectively. The metrology system can be a noncontact (e.g., laser-based) or contact system (e.g., string–pot-based [12]) that measures the relative location of the material deposition tool to a known location for accurate placement of material from the deposition tool. The material supply system feeds the deposition tool with concrete or other material. It can be a cement truck or hopper, as shown in Fig. 2, with a pump to move material to the tool. The material supply and the metrology subsystems will employ commercial products where possible. Fig. 3 shows an experiment at NIST in (manual) deposition of concrete, building a portion of a wall via a prototype deposition nozzle with slip-form tool. Such deposition nozzles are also available commercially (e.g., www.curbequipment.com; www.basin-gallant.com/concretecurbsidewalk.html).[1]

One good choice for the Cartesian metrology system is a series of three noncontact lasers aimed at the crane deposition system (Fig. 2). This solution provides an accurate 6-*dof* (degrees of freedom) pose

[1] The identification of any commercial product or trade name does not imply endorsement or recommendation by Ohio University or NIST.

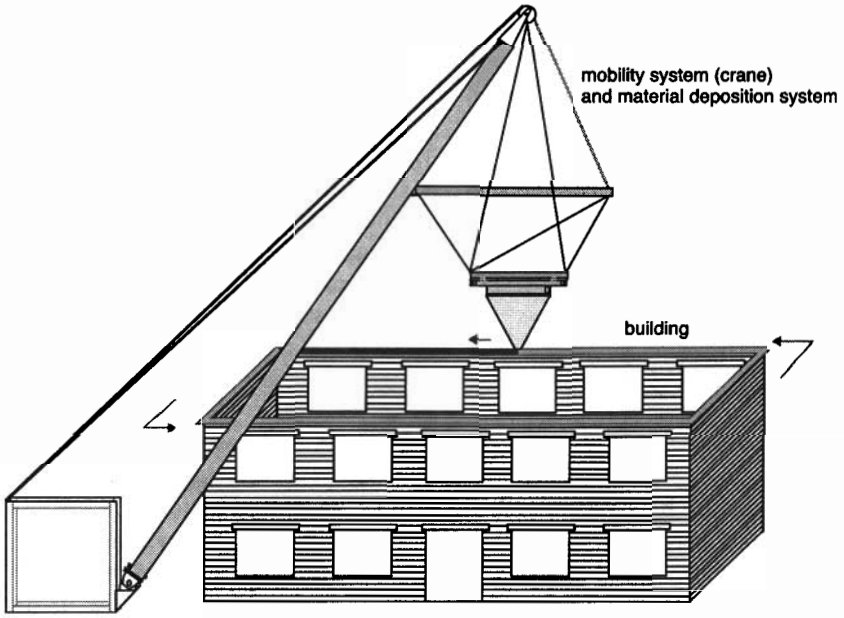

Fig. 1. Automated construction system.

measurement that is independent of the drive train encoders for cable length feedback.

Now, we present an estimate of the time required to build a nominal house [15.2 × 9.1 × 6.1 m (50 × 30 × 20 ft)], via manual methods in this paragraph, followed by the automated system in the following paragraph. Typical of today's construction methods are labor-intensive block and brick placement with mortar joints. Assuming standard block dimensions 0.2 × 0.2 × 0.4 m (8 × 8 × 16 in), there will be 120 blocks per layer and 30 layers in the house. Assuming 20 s for laying and mortaring each block, 20 h is required to lay the blocks for the entire house. Then, assuming a postprocess stucco application time of 32.3 s/m^2 (3 s/ft^2), an additional 2.7 h is required for surface finishing.

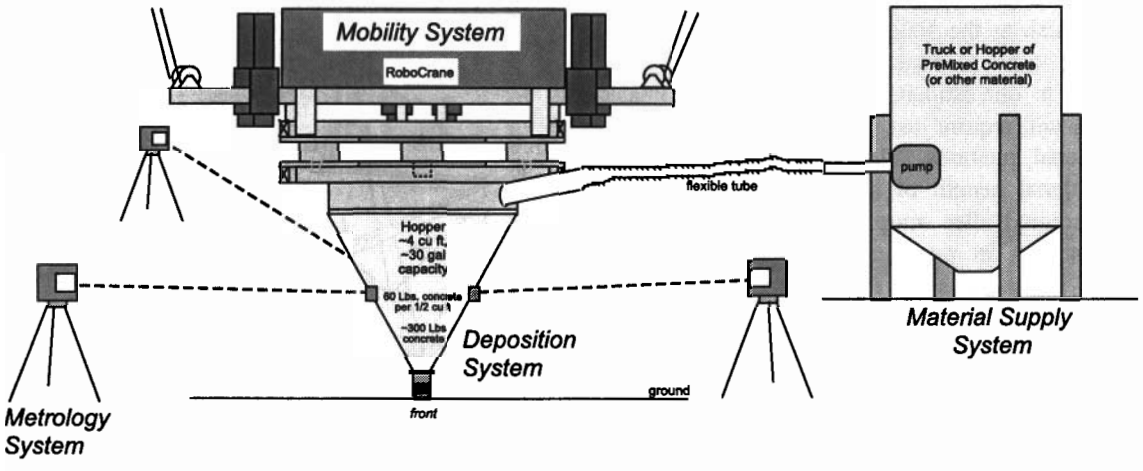

Fig. 2. Automated construction subsystems.

Fig. 3. NIST concrete deposition experiment.

Thus, we estimate almost 23 h (22 h, 40 min) is required for blocking the house via conventional manual methods.

Now, we estimate the time required for building an equivalent structure via concrete deposition using the proposed automated construction system instead of manual block-laying. Current concrete slip-form technology (e.g., www.curbmate.com)[1] enables large block-sized [cross section of 0.13×0.2 m (5×8 in)] deposition of concrete at a rate of 4.9 m/min (16 ft/min). For the same nominal $15.2 \times 9.1 \times 6.1$ m house, using this deposition cross section, 48.8 m (160 ft) travel is required per row, with 48 rows required. Therefore, the total deposition travel must be 2340.9 m (7680 ft), and the total deposition time is thus 8 h. Because the automated system can be designed to apply the desired finish as the walls are being constructed, no additional time is required for finishing. Thus, according to our estimates, the proposed automated approach will require just over one-third the time of conventional methods. The automated system has the additional benefit of little to no human supervision required after setup.

Not shown in our simple estimates are other required processes such as reinforcement between layers (one reinforcement process is explained in Ref. [7]). Also not shown in the estimate are embedded processes that could be installed during the wall-build process, such as water piping and heat ducts, plus electrical, phone, Internet, and other utilities. With single block-sized layers, these utilities could be installed within the concrete layers; we can also develop an autonomous dual-wall approach for this.

3. Mobility system

This section presents the description, kinematics, and statics for the self-contained cable-suspended robot of Fig. 1. This is the mobility subsystem of our overall automated construction system concept.

3.1. Mobility system description

Fig. 4 shows the NIST self-contained mobility subsystem concept. This robot is intended to be a versatile, economic, accurate tool for the construction industry. The system is supported by a standard construction site dumpster, fitted with moment resisting support rods to resist tipping; the dumpster is rotated by a small angle ϕ_B to move the tipping point forward from the front edge of the dumpster.

In Fig. 4, the fixed base frame has fixed cable connection points B_1, B_2, B_3, and B_4. The moving mast (boom C_1B_0 plus hinged equilateral triangle $C_2C_3C_4$) is connected to the base dumpster via a universal joint (allowing pitching and yawing) at B_0. The moving mast is articulated via cables of lengths L_{B1} and L_{B2}, whose active actuating winches are mounted at points B_1 and B_2. Therefore, vertical cable support point C_1 can move to increase the system workspace in a self-contained manner. Points B_1 and

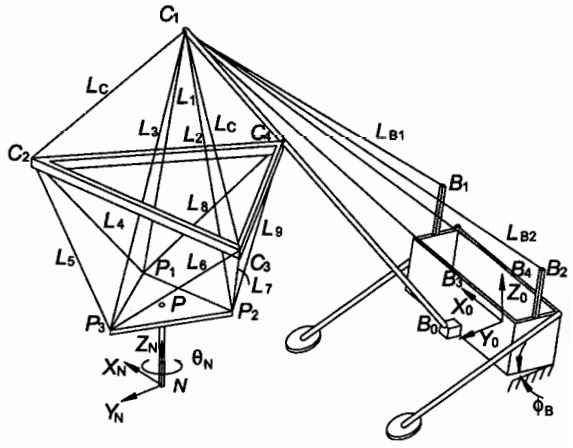

Fig. 4. NIST automated construction system diagram.

B_2 are assumed to lie on the right and left dumpster sides, but can be mounted anywhere along these sides, and above the top of the dumpster as shown. Two passive, fixed-length cables support the equilateral triangle, attached from fixed point B_4 over pulleys at point C_1 to moving points C_2 and C_3. The vertices of the moving platform are P_1, P_2, and P_3, and point P is the centroid of the moving platform. The deposition nozzle tip N is located at the origin of moving frame $\{N\}$. Because RoboCrane-type devices have limited rotations, the entire nozzle is rotated via a turntable attached to the moving platform, with rotary variable θ_N. The world coordinate frame $\{0\}$ is aligned with the floor at the back edge of the dumpster as shown; this frame is really hidden in the view of Fig. 4.

The lengths of the nine additional active cables are L_i, $i=1,2,\ldots,9$. As shown in Fig. 4, cable 1 connects C_1 to P_1, cable 2 connects C_1 to P_2, cable 3 connects C_1 to P_3, cable 4 connects C_2 to P_1, cable 5 connects C_2 to P_3, cable 6 connects C_3 to P_3, cable 7 connects C_3 to P_2, cable 8 connects C_4 to P_1, and cable 9 connects C_4 to P_2. Cable lengths 1, 2, and 3 are controlled by active winches mounted at B_3; therefore, the line B_3C_1 is actually three (articulating because C_1 can move) cables, passing from each winch over point C_1 to moving platform point P_i, $i=1,2,3$; these three are the heavy-lift cables. Cables 4 and 5 are controlled by active winches mounted at C_2, cables 6 and 7 are controlled by active winches mounted at C_3, and cables 8 and 9 are controlled by active winches mounted at C_4. Cables 4–9 provide stable, rigid control of all 6 degrees of freedom in conjunction with the heavy-lift cables.

The concept of Fig. 4 can be seen as an irregular RoboCrane with moving, self-contained, vertical support points C_1, C_2, C_3, and C_4, controlled by cables 1 through 9. This RoboCrane, however, is overactuated (three more cables than the minimum number of six cables for a ceiling-mounted RoboCrane and 6-*df* operation). Points C_2 and C_3 allow the moving platform workspace to extend beyond vertical point C_1. To maintain control in all motions, all cable tensions must remain positive at all times.

In order to provide a more stable standard construction site dumpster base, we tilt the base by a small angle ϕ_B about the X_0 axis on the back bottom corner of the dumpster (see Fig. 4). This moves the tipping point of the system from the front bottom corner of the dumpster to the end of the moment resisting rods of length d_M. As shown in Fig. 5, the mechanism analogy for this dumpster tipping is a slider–crank mechanism, where the crank d_{B3} pivots about X_0, the coupler is d_M (hinged at the back top corner of the dumpster), and the foot pad (spreading out the weight over the ground) is the slider, connected to d_M with a pin joint. From this slider–crank analogy, given the desired dumpster tilting angle ϕ_B, we can calculate the variables ϕ_M and y_M (same for both dumpster sides at different X_0 locations).

$$\phi_M = \cos^{-1}\left(\frac{d_{B3}\cos\phi_B}{d_M}\right) - \phi_B$$

$$y_M = d_M\sin(\phi_M + \phi_B) - d_{B3}\sin\phi_B \quad (1)$$

The dumpster tilting in Fig. 5 could be actuated by cables and winches, one set on either side of the dumpster, where the motor and winch is mounted to the dumpster and the other end of the cable is mounted to the coupler d_M (or vice versa).

3.2. Mast subsystem kinematics

This section presents the kinematics analysis for the mast portion of the NIST Automated Construction System. We wish the equilateral triangle to be as horizontal as possible for all motion.

The role of the mast is to provide self-contained mobility for the RoboCrane-like portion of the automated construction system (see Fig. 4). As shown in Fig. 6, the mast consists of equilateral triangle $C_2C_3C_4$ hinged via a revolute joint to boom C_1B_0 at point C_4.

The key aspect of this mast concept is that the configuration of the equilateral triangle portion is maintained by two fixed-length, passive cables. Both cables are fixed to the dumpster at point B_4, pass over pulleys at point C_1, and are fixed to moving equilateral triangle points C_2 and C_3. As cables L_{B1} and L_{B2} move

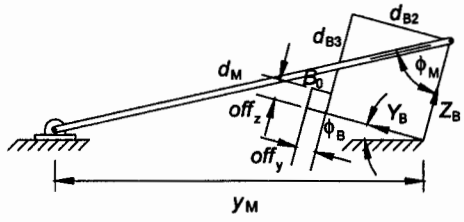

Fig. 5. Slider–crank analogy for dumpster tipping.

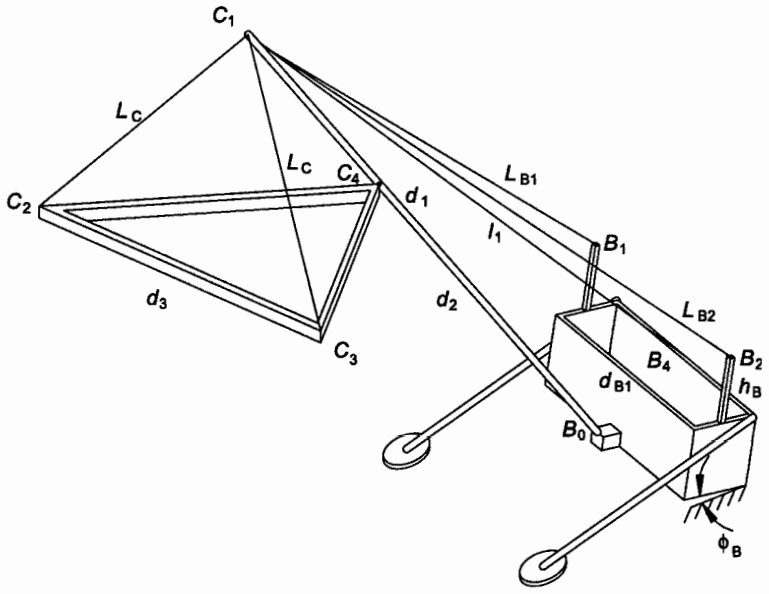

Fig. 6. Mobility system mast.

point C_1, these passive cables move and support the equilateral triangle portion passively, which in turn supports six of the RoboCrane-like cables for moving the automated construction platform. At any instant during motion, the two passive cables can be seen as two lengths on either side of the pulley, L_C between point C_1 and points C_2 and C_3, respectively, and l_1 between moving point C_1 and fixed point B_4. With this design, having a revolute joint at C_4 (whose axis is aligned with X_0 and X_B in the nominal configuration when the boom is in the Y_0Z_0 plane), both cable portions L_C are guaranteed to be (theoretically) the same length for all motion, which ensures that the Z components of C_2 and C_3 are always the same (although different from the Z component of C_4 in general). This passive motion control for the equilateral triangle portion of the mast enables a pantograph-like motion. L_C and l_1 both change during motion, but their sum is constant, set by design to keep the equilateral triangle as horizontal as possible during all motion.

Fig. 7 shows a kinematic diagram of the mast, connected to the dumpster frame at point B_0 via a universal joint allowing yaw (θ_1) and pitch (θ_2). This reference position defines both angles to be zero. The mast can be considered to be a 3R serial robot connected to the dumpster with joint angles θ_1 and θ_2, plus angle θ_3 moving the triangle with respect to the boom. θ_1, θ_2, and θ_3 are not controlled directly but via active cables L_{B1} and L_{B2}, and passive cables L_C+l_1. The origin of frame $\{B_0\}$ is mounted to point B_0; the orientation of $\{B_0\}$ is identical to that of $\{B\}$ (which is the same as $\{0\}$ but rotated by ϕ_B).

As seen in Fig. 7, d_1 is the length of boom C_1B_0, d_2 is the length from boom base point B_0 to the equilateral triangle connection point C_4, and d_3 is the

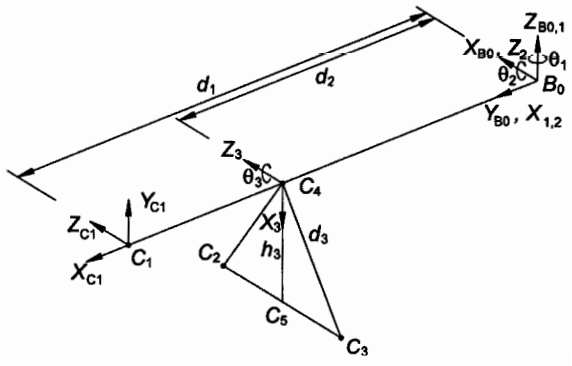

Fig. 7. Mast kinematic diagram.

Table 1
Mast Denavit–Hartenberg parameters

i	α_{i-1}	a_{i-1}	d_i	θ_i
1	0	0	0	$\theta_1+90°$
2	90°	0	0	θ_2
3	0	d_2	0	θ_3

equilateral triangle side (with height h_3). Moving point C_5 is the midpoint of C_2C_3.

The pitch angle θ_2 should be kept well away from the ground position because this approaches a singularity where cables L_{B1} and L_{B2} are collinear with the mast; *in this singularity, infinite force would be* required to move the mast (due to the system design, the singularity actually occurs underground, but high forces are required as the mast approaches the ground). In setup, the boom will most likely be lifted by these cables from the ground; thus, this is another reason to mount points B_1 and B_2 above the dumpster top by h_B (this effectively moves the singularity further from the ground).

The Denavit–Hartenberg (DH) parameters [5] for this serial robot are given in Table 1. Note that a joint angle offset of 90° is required for $i=1$ (i.e., $\theta_1+90°$) because the X_{B0} and X_1 axes are not aligned in the zero position. Note also that, in the convention of Ref. [5], the only mast length parameter to appear in the DH table is d_2 because the last active frame is {3}, centered at C_4. The other pertinent lengths must be included at the next stage of mast kinematics. In Table 1, θ_i are the only variables, while the remaining DH parameters are constant.

The homogeneous transformation matrices relating frames $\{C_i\}$, $i=2,3,4,5$ (whose origins are points C_i and whose orientation is identical to that of {3}), to the world frame $\{B_0\}$ can be found using symbolic computer kinematics from the DH parameters and homogeneous transformation relationships.

$$\left[{}^{B_0}_{C_i}\mathbf{T}\right] = \left[{}^{B_0}_{1}\mathbf{T}(\theta_1)\right]\left[{}^{1}_{3}\mathbf{T}(\theta_2,\theta_3)\right]\left[{}^{3}_{C_i}\mathbf{T}\right] \quad i=2,3,4,5 \quad (2)$$

Note that in Eq. (2), we have taken advantage of the consecutive parallel $\hat{Z}_2$ and $\hat{Z}_3$ axes; in such cases, we expect functions of $(\theta_2+\theta_3)$ to simplify the kinematics equations via sum-of-angle formulas. The last transforms $\left[{}^{3}_{C_i}\mathbf{T}\right]$ for use in Eq. (2) are obtained by using identity for the orientation and the constant relative position vectors $\{{}^3\boldsymbol{C}_i\}$. Substituting the DH parameters and the constant transforms into Eq. (2) yields:

$$\left[{}^{B_0}_{C_4}\mathbf{T}\right] = \begin{bmatrix} -s_1c_{23} & s_1s_{23} & c_1 & -d_2s_1c_2 \\ c_1c_{23} & -c_1s_{23} & s_1 & d_2c_1c_2 \\ s_{23} & c_{23} & 0 & d_2s_2 \\ 0 & 0 & 0 & 1 \end{bmatrix} \quad (3)$$

where we have used the abbreviations $c_i=\cos\theta_i$ and $s_i=\sin\theta_i$; furthermore, $c_{23}=\cos(\theta_2+\theta_3)$ and $s_{23}=\sin(\theta_2+\theta_3)$. The formula for $\{{}^{B_0}\boldsymbol{C}_4\}$ is the fourth column, first three rows of Eq. (3). Other position vectors are:

$$\{{}^{B_0}\boldsymbol{C}_1\} = \begin{Bmatrix} -d_1s_1c_2 \\ d_1c_1c_2 \\ d_1s_2 \end{Bmatrix} \qquad \{{}^{B_0}\boldsymbol{C}_2\} = \begin{Bmatrix} -d_2s_1c_2 - h_3s_1c_{23} + \frac{d_3}{2}c_1 \\ d_2c_1c_2 + h_3c_1c_{23} + \frac{d_3}{2}s_1 \\ d_2s_2 + h_3s_{23} \end{Bmatrix}$$

$$\{{}^{B_0}\boldsymbol{C}_3\} = \begin{Bmatrix} -d_2s_1c_2 - h_3s_1c_{23} - \frac{d_3}{2}c_1 \\ d_2c_1c_2 + h_3c_1c_{23} - \frac{d_3}{2}s_1 \\ d_2s_2 + h_3s_{23} \end{Bmatrix} \qquad \{{}^{B_0}\boldsymbol{C}_5\} = \begin{Bmatrix} -d_2s_1c_2 - h_3s_1c_{23} \\ d_2c_1c_2 + h_3c_1c_{23} \\ d_2s_2 + h_3s_{23} \end{Bmatrix} \quad (4)$$

The orientation associated with $\{^{B_0}\boldsymbol{C}_1\}$ is not dependent on θ_3:

$$[{}^{B_0}_{C_1}\mathbf{R}] = \begin{bmatrix} -s_1c_2 & s_1s_2 & c_1 \\ c_1c_2 & -c_1s_2 & s_1 \\ s_2 & c_2 & 0 \end{bmatrix} \quad (5)$$

Now, given values for θ_1, θ_2, and θ_3, it is easy to evaluate the absolute position of moving points C_i with respect to $\{B_0\}$ using the above formulas. Ultimately, all vectors will be represented in the $\{0\}$ frame using ${}^0_{C_i}\mathbf{T} = {}^0_{B_0}\mathbf{T}\,{}^{B_0}_{C_i}\mathbf{T}$. However, these serial angular values θ_1, θ_2, and θ_3 will not be known because it would increase cost and complexity unnecessarily to add angle sensing to the passive universal joint at B_0 and passive revolute joint at C_4. Instead, we have two choices.

(1) For inverse pose kinematics, the upper mast point C_1 is specified at each instant (it can be moving). It is convenient to specify C_1 via angles θ_1 and θ_2 (because C_1 is constrained by the length d_1), using the first expression of (4). If we wish to specify the pitch angle as an absolute (horizontally referenced) angle, we need to calculate first the relative pitch angle using the dumpster tilting angular offset: $\theta_2 = \theta_{2\mathrm{ABS}} - \phi_B$. Then, we can easily calculate the two required cable lengths L_{B1} and L_{B2} using the Euclidean norm of the appropriate vector differences as given below:

$$L_{B1} = \|{}^0\boldsymbol{C}_1 - {}^0\boldsymbol{B}_1\| \quad L_{B2} = \|{}^0\boldsymbol{C}_1 - {}^0\boldsymbol{B}_2\| \quad (6)$$

(2) For forward pose kinematics, the two cable lengths, L_{B1} and L_{B2}, are known from their winch angular feedback measurements. Upper mast point C_1 is calculated given these two cable lengths. From Figs. 4 and 6, point C_1 is the intersection of three spheres: fixed mast radius d_1 centered at B_0, radius L_{B1} centered at B_1, and radius L_{B2} centered at B_2. The intersection of three spheres is also the basis for the forward pose kinematics solution of the nine-cable RoboCrane-like device. This solution is presented in Ref. [12]. ${}^0\boldsymbol{C}_1$ is found from the intersection of three spheres with these center and radii: $({}^0\boldsymbol{B}_1, L_{B1})$, $({}^0\boldsymbol{B}_2, L_{B2})$, and $({}^0\boldsymbol{B}_0, d_1)$. Note that this ordering of the three spheres is very important to avoid singularities [12]. Given ${}^0\boldsymbol{C}_1$, we next calculate this vector with respect to $\{B_0\}$: ${}^{B_0}\boldsymbol{C}_1 = [{}^0_{B_0}\mathbf{T}^{-1}]\,{}^0\boldsymbol{C}_1$; then, we can calculate passive universal joint angles θ_1 and θ_2 from an inverse position kinematics solution of the expression for $\{^{B_0}\boldsymbol{C}_1\} = \{P_x\ P_y\ P_z\}^T$ in Eq. (4):

$$\theta_1 = \tan^{-1}\left(\frac{-P_x}{P_y}\right) \quad \theta_2 = \sin^{-1}\left(\frac{P_z}{d_1}\right) \quad (7)$$

Note that the resulting θ_2 in Eq. (7) is a relative angle with respect to $\{B_0\}$; the absolute (horizontally referenced) pitch angle must take dumpster tilting angle ϕ_B into account: $\theta_{2\mathrm{ABS}} = \theta_2 + \phi_B$.

Now, we can determine θ_3; it is done in the same manner for both of the above cases. Note that θ_3 is defined to be a relative angle (with respect to boom C_1B_0) and hence requires no offset like θ_2. Fig. 8 shows a side view of the mast arrangement. This side view shows a planar representation of the passive equilateral triangle pantograph cables; $l_1 = \|C_1B_4\|$ are the real portions of the two passive pantograph cables, and $l_2 = \|C_1C_5\|$ is a virtual variable cable representing the planar projections of the cables' portions L_C (see Fig. 6 and visualize the plane $C_1C_2C_3$; l_2 bisects this triangle): $l_2 = \sqrt{(L_C^2 - d_3^2)/4}$. Then, using the *law of cosines*:

$$\theta_3 = -\cos^{-1}\left[\frac{h_3^2 + (d_1 - d_2)^2 - l_2^2}{2h_3(d_1 - d_2)}\right] \quad (8)$$

θ_3 is negative in Eq. (8) due to its definition in Figs. 7 and 8. This pantograph mechanism is designed to attempt to maintain the equilateral triangle as near

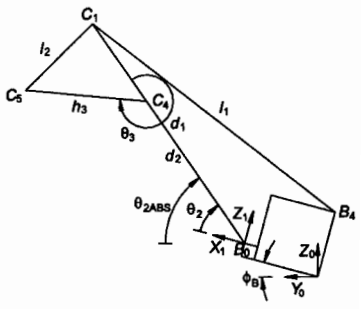

Fig. 8. Mast side view.

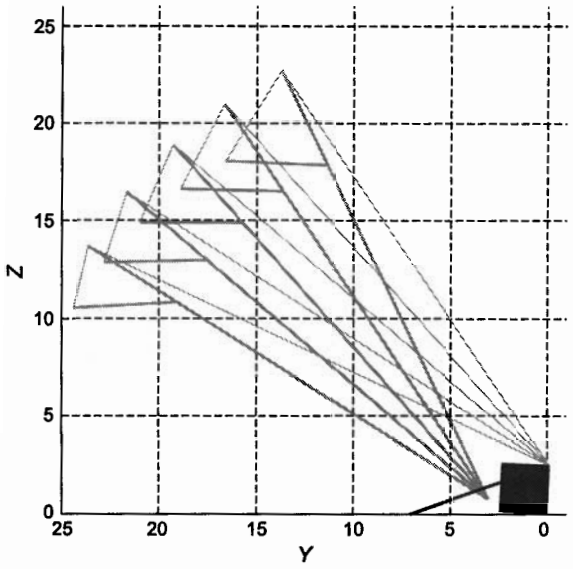

Fig. 9. Passive horizontal mechanism demonstration.

horizontal as possible for all motion. It can be exact only at one θ_2 angle, but we wish it to be close at all other configurations. If the triangle is perfectly horizontal, the following condition is met: $\theta_3 = -\theta_{2ABS}$.

Now, we still need to calculate the (actual) cable lengths L_C for θ_3 determination. The two passive pantograph cables (running from B_4, over pulleys at C_1, connecting to points C_2 and C_3) are of fixed length, $L_{nom} = l_1 + L_C$. Therefore, $L_C = L_{nom} - l_1$. Let us fix L_{nom} by design, requiring the equilateral triangle to be exactly horizontal ($\theta_3 = -\theta_{2ABS}$) at a nominal value of the absolute pitch angle ($\theta_{2ABSnom}$) and for the central value of the yaw angle, $\theta_{1nom} = 0$; $\theta_{2ABSnom}$ should be in the middle of the allowable θ_{2ABS} range, or some other nominal, often-used configuration. At the nominal configuration, we have $L_{nom} = l_{1nom} + L_{Cnom}$, where $l_{1nom} = \| C_{1nom}B_4 \|$. We also have $L_{Cnom} = \sqrt{(l_{2nom}^2 + d_3^2)/4}$; the nominal virtual pantograph cable length is $l_{2nom} = \| C_{1nom}C_{5nom} \|$. The nominal locations of C_1 and C_5 are found by substituting $\theta_1 = 0$ and relative angle $\theta_{2nom} = \theta_{2ABSnom} - \phi_B$ into the first and last expressions of Eq. (4):

$$\{{}^{B_0}C_{1nom}\} = \begin{Bmatrix} 0 \\ d_1 c_{2nom} \\ d_1 s_{2nom} \end{Bmatrix} \quad \{{}^{B_0}C_{5nom}\} = \begin{Bmatrix} 0 \\ d_2 c_{2nom} + h_3 c\phi_B \\ d_2 s_{2nom} - h_3 s\phi_B \end{Bmatrix} \tag{9}$$

Finally, given θ_1, θ_2, and θ_3 from Eqs. (7) and (8), we can calculate the position vectors for points C_i from Eq. (4), for general configurations; we can then transform these to $\{0\}$.

Our current mobility system parameters are (in m) $d_M = 7.620$, $d_1 = 24.384$, $d_2 = 18.999$, $d_3 = 6.096$, $\text{off}_y = \text{off}_z = 0.6096$, and $\phi_B = 3°$. We assume a standard $6.096 \times 2.438 \times 2.438$ base dumpster; points B_1 and B_2 are at the front of the dumpster, mounted $h_B = 2.438$ from the dumpster top. Fig. 9 shows a series of mast motions in the Y_0Z_0 plane for our mast design.

Fig. 10 shows the horizontality results for our mast design, over all motion. Mast pitch angle θ_{2ABS} is the independent variable, while families of curves are given for different θ_1 values (0°, 15°, 30°, 45°); in this manner, one plot covers all motion. Note that in all results (including statics later), the motion is symmetric with respect to $\pm\theta_1$.

Fig. 10 shows the $-\theta_3$ results (negative for easy comparison to the mast pitch angle θ_2) for all motion. For horizontality, we desire $\theta_3 = -\theta_{2ABS}$, which is the dashed (Ideal) line in Fig. 10. We can see that this is satisfied (theoretically) only at $\theta_{2ABS} = -\theta_{2ABSnom} = 48°$, for $\theta_1 = 0$. Away from this condition, the $-\theta_3$ results deviate significantly from the desired dashed line.

Fig. 11a shows the X_0Y_0 workspace and Fig. 11b shows its associated C_2C_3 Z_0 heights, for our mast

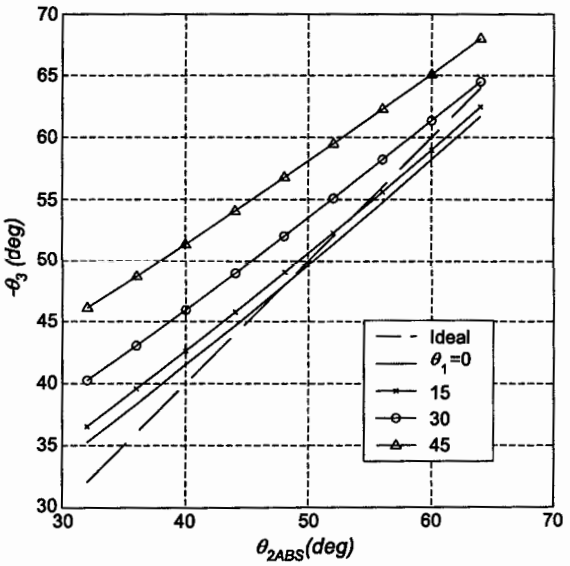

Fig. 10. Mast angle θ_3.

design for all motion. In analyses with different mast designs, we discovered that good horizontality is associated with poor X_0Y_0 workspace and vice versa, demonstrating tradeoffs between performance measures in mast design.

3.3. Mobility system kinematics

The inverse pose kinematics problem is stated: given the required nozzle tip pose $[{}^0_N\mathbf{T}]$ and the desired position of upper mast point ${}^0\boldsymbol{C}_1$, calculate the 11 cable lengths L_i, $i=1,2,\ldots,9$ and L_{B1} and L_{B2} and θ_N. The solution to this problem may be used as the basis for a pose control scheme. For the automated construction system, inverse pose kinematics is easier to solve than forward pose kinematics: given the pose of the nozzle tip $\{N\}$ tool, we first specify θ_N according to deposition task requirements. Then, we can find moving platform cable connection points P_1, P_2, and P_3; then, the inverse pose solution consists simply of calculating the cable lengths using the Euclidean norm of the appropriate vector differences between the various moving and fixed cable connection points. The inverse pose kinematics solution yields a unique closed-form solution, and the computation requirements are not demanding.

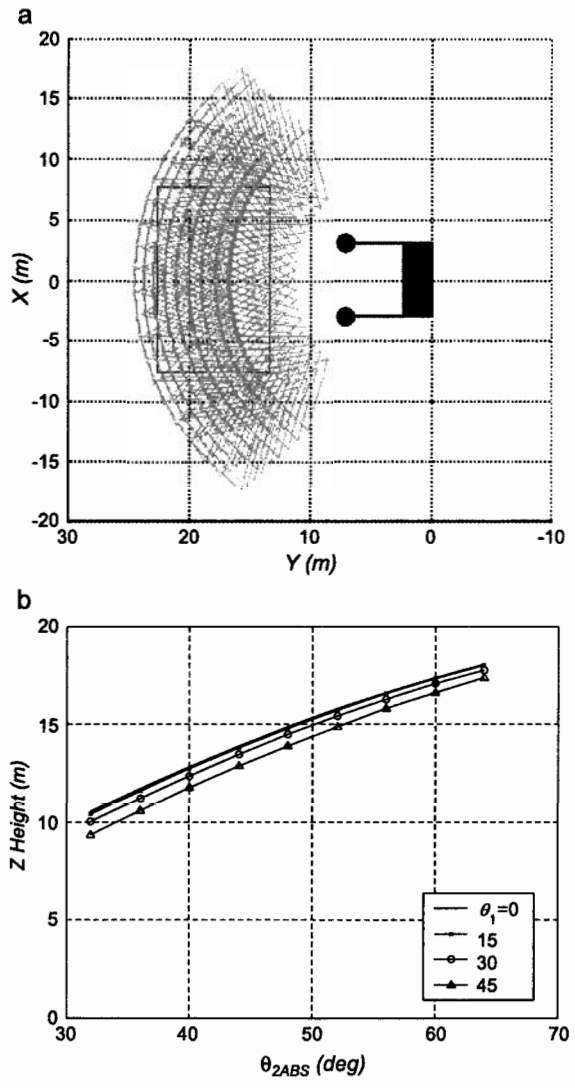

Fig. 11. (a) Mast X_0Y_0 workspace projection. (b) Associated Z_0 heights.

As presented in Section 3.2, the first steps in the inverse pose kinematics solution are to specify C_1 via angles θ_1 and θ_2 using Eq. (4), calculate L_{B1} and L_{B2} using Eq. (6), calculate θ_3 from Eq. (8), and then calculate the remaining moving cable-connection points C_i using Eqs. (3) and (4). With an alternate telescoping boom design, it is possible to easily specify C_1 directly and then calculate angles θ_1 and θ_2.

Given $[{}^0_N\mathbf{T}]$ and θ_N, we then calculate the moving platform pose $[{}^0_P\mathbf{T}]$ and then moving cable connection points P_1, P_2, and P_3: $[{}^0_P\mathbf{T}]=[{}^0_N\mathbf{T}][{}^P_N\mathbf{T}]^{-1}$, where ${}^P_N\mathbf{T}$ is a function of θ_N and the nozzle position with respect to the moving platform. The vector positions of points P_i with respect to $\{0\}$ are:

$$\{{}^0\boldsymbol{P}_i\} = [{}^0_P\mathbf{T}]\{{}^P\boldsymbol{P}_i\} \qquad i=1,2,3 \tag{10}$$

Note that we must augment each position vector in (1.0) with a '1' in the fourth row. The fixed relative vectors $\{{}^P\boldsymbol{P}_i\}$ are from platform geometry. Given the moving cable connection points P_1, P_2, and P_3 in $\{0\}$ from Eq. (10), we can find the nine unknown cable lengths. The inverse pose kinematics solution is the Euclidean norm of the appropriate vector differences as shown below:

$$\begin{aligned} L_1 &= \|{}^0P_1 - {}^0C_1\| \quad L_2 = \|{}^0P_2 - {}^0C_1\| \quad L_3 = \|{}^0P_3 - {}^0C_1\| \\ L_4 &= \|{}^0P_1 - {}^0C_2\| \quad L_5 = \|{}^0P_3 - {}^0C_2\| \quad L_6 = \|{}^0P_3 - {}^0C_3\| \\ L_7 &= \|{}^0P_2 - {}^0C_3\| \quad L_8 = \|{}^0P_1 - {}^0C_4\| \quad L_9 = \|{}^0P_2 - {}^0C_4\| \end{aligned} \tag{11}$$

The forward pose kinematics solution is required for simulation and sensor-based control of the NIST Au-

tomated Construction Mobility System. The forward pose kinematics problem is stated: given the 11 cable lengths L_i, $i=1,2,\ldots,9$, and L_{B1}, L_{B2}, and θ_N, calculate the nozzle tip pose $\lfloor {}^0_N\mathbf{T}\rfloor$. For this system, forward pose kinematics is not as straightforward as inverse pose kinematics. However, unlike most parallel robot forward pose kinematics problems, there exists a closed-form solution, and the computation requirements are not demanding. There are multiple solutions, but, generally, the correct solution for the automated construction system can be easily determined.

As presented in Section 3.2, the first steps in the forward pose kinematics solution are to calculate C_1 given L_{B1} and L_{B2} using the intersection of three spheres, calculate the passive universal joint angles θ_1 and θ_2 from Eq. (7), calculate θ_3 from Eq. (8), and then calculate the remaining moving cable-connection points C_i using Eqs. (3) and (4). The remaining forward pose kinematics solution consists of finding the intersection point of three given spheres; this must be done three additional times in the following sequence, one for each moving platform cable connection point P_i. Let us refer to a sphere as a vector center point $\boldsymbol{c}$ and scalar radius r: $(\boldsymbol{c},r)$.

1. P_1 is found from the intersection of: $({}^0\boldsymbol{C}_2,L_4)$, $({}^0\boldsymbol{C}_4,L_8)$, $({}^0\boldsymbol{C}_1,L_1)$.
2. P_2 is found from the intersection of: $({}^0\boldsymbol{P}_1,d_p)$, $({}^0\boldsymbol{C}_4,L_9)$, $({}^0\boldsymbol{C}_1,L_2)$.
3. P_3 is found from the intersection of: $({}^0\boldsymbol{P}_1,d_p)$, $({}^0\boldsymbol{P}_2,d_p)$, $({}^0\boldsymbol{C}_1,L_3)$.

The detailed solution for the intersection of three spheres is presented in Ref. [12]; that reference also presents discussions on imaginary solutions, singularities, and multiple solutions. Now, let us finish the forward pose kinematics solution. Given ${}^0\boldsymbol{P}_i$, we can calculate the orthonormal rotation matrix $\lfloor {}^0_P\mathbf{R}\rfloor$ directly, using the definition that each column of this matrix expresses one of the XYZ unit vectors of $\{P\}$ with respect to $\{0\}$ [5]. These columns are calculated as follows, from moving platform geometry.

$$
{}^0\hat{X}_P = \frac{{}^0\boldsymbol{P}_1 - {}^0\boldsymbol{P}_2}{\|{}^0\boldsymbol{P}_1 - {}^0\boldsymbol{P}_2\|} \qquad {}^0\hat{Y}_P = \frac{{}^0\boldsymbol{P}_3 - {}^0\boldsymbol{P}_4}{\|{}^0\boldsymbol{P}_3 - {}^0\boldsymbol{P}_4\|}
$$
$$
{}^0\hat{Z}_P = {}^0\hat{X}_P \times {}^0\hat{Y}_P \tag{12}
$$

where ${}^0\boldsymbol{P}_4$ is the midpoint of P_1P_2. Given ${}^0\boldsymbol{P}_i$ and $\lfloor {}^0_P\mathbf{R}\rfloor$, we then have $\lfloor {}^0_P\mathbf{T}\rfloor$, and $[{}^0_P\mathbf{T}]=[{}^0_{P_i}\mathbf{T}][{}^P_{P_i}\mathbf{T}]^{-1}$. Finally, use $\lfloor {}^0_N\mathbf{T}\rfloor=\lfloor {}^0_P\mathbf{T}\rfloor\lfloor {}^P_N\mathbf{T}\rfloor$ to calculate the nozzle tip pose.

There are two solutions to the intersection point of three given spheres [12]; therefore, the forward pose kinematics problem yields a total of $2^4=16$ mathematical solutions because we must repeat the algorithm four times for the NIST Automated Construction Mobility System. It is generally straightforward to determine the correct solution using logic in the forward pose kinematics software. Fig. 12 shows a nominal pose for our mobility system design Matlab simulation.

3.4. Mast subsystem statics

This section discusses the model for quasi-static tension-based control of the cable-suspended construction system. We first consider mast-moving tensions, then the overall mast statics model, followed by simulation results.

3.4.1. Mast-moving tensions

Now, we consider a crucial issue for moving the mast. If the yaw angle θ_1 is commanded to a value that is very large, one of the mast-moving cables will require an impossible pushing force. Fig. 13 shows the top view of these mast-moving cables plus boom. When the X_0Y_0 projection of mast B_0C_1 becomes

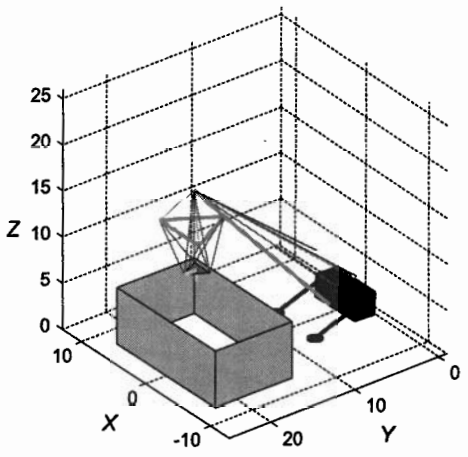

Fig. 12. Mobility system Matlab model.

collinear with the X_0Y_0 projection of cable L_{B1}, we have reached the positive limit on θ_1 (by symmetry, the equal, negative limit on θ_1 occurs when B_0C_1 is collinear with L_{B2}). We can calculate $\pm\theta_{1LIMIT}$ as follows:

$$\pm\theta_{1LIMIT} = \pm\tan^{-1} \times \left[\frac{d_{B1}/2}{(d_{B2}(1-f_2)+\text{off}_y)\cos\phi_B + (d_{B3}+h_B-\text{off}_z)\sin\phi_B}\right]$$

f_2 is the fraction along the Y_B direction where points B_1 and B_2 are mounted to the dumpster. Fig. 14 shows θ_{1LIMIT} for f_2 fractions from 0 to 1 and different dumpster tipping angle values $\phi_B = 1°, 3°, 5°, 7°$.

We see that $\pm\theta_{1LIMIT}$ increases (which is good) with increasing f_2 in all cases; furthermore, $\pm\theta_{1LIMIT}$ decreases (which is bad) with increasing ϕ_B in all cases. Any specific design is a single point on Fig. 14; the plots verify that, for large limits on θ_1, we must move the points B_1 and B_2 as far forward as possible ($f_2 = 1$). However, this causes a loss of half the moment arm for lifting the mast (compared to $f_2 = 0$); this is why we also raised B_1 and B_2 off the dumpster in the Z_B direction an additional h_B amount, to recover the original moment arms for cables L_{B1} and L_{B2}. All motion should be kept well away from the specific $\pm\theta_{1LIMIT}$ for any given design, to safely avoid the slack cable problem and the resulting catastrophic loss of control. For our design with $\phi_B = 3°$, the theoretical θ_1 limit is $\pm$ 74.7°.

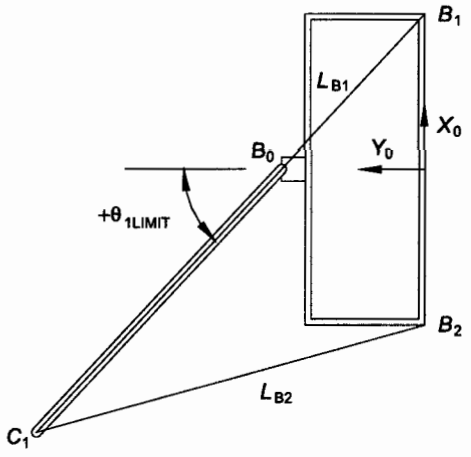

Fig. 13. θ_{1LIMIT} determination.

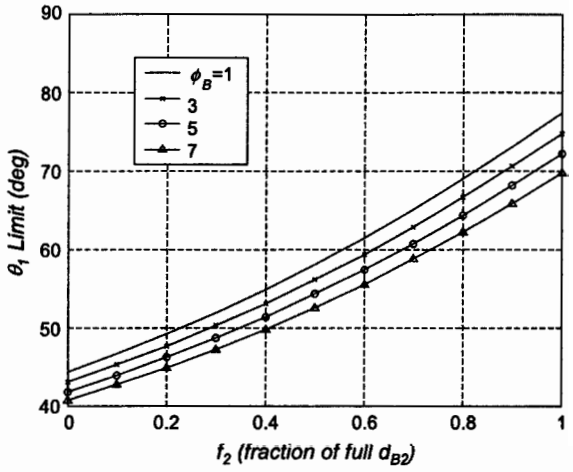

Fig. 14. θ_{1LIMIT} for different ϕ_B, f_2.

3.4.2. Mast statics model

The mast statics problem is stated: given external loads at points C_i, $i = 1,2,3,4$, plus the system configuration, calculate the tensions in all cables. Internal joint forces between rigid members are also unknown. We assume all crane members are weightless and all cables are in tension. Now, we outline our general 3D mast statics solution. For each of the free body diagrams (not shown due to lack of space) of the equilateral triangle $C_2C_3C_4$, pantograph pulley, and boom B_0C_1, we can write two 3D vector equations of static equilibrium: $\Sigma\boldsymbol{F} = 0$ and $\Sigma\boldsymbol{M} = 0$. Therefore, we have a total of six scalar equations times three moving bodies, for 18 equations. However, we only have 12 unknowns, scalar cable tensions t_C (the same for both passive pantograph cables), t_{B1}, and t_{B2} (the active mast-moving cable tensions), plus three 3D vector internal force unknowns, between the equilateral triangle and boom, between the pulley and boom, and between the boom and base dumpster. Thus, for solution, we ignore six of the statics equations; if we follow the method now described, the unknowns may be found member by member. Firstly, for the equilateral triangle, use only the $\Sigma M_z = 0$ scalar equation, in {3} coordinates; this equation yields the unknown t_C, the tension in both pantograph cables C_1C_2 and C_1C_3. Then, we use all three force components in the $\Sigma\boldsymbol{F} = 0$ vector equation to find the internal force of the boom acting on the equilateral triangle at the pin joint located at C_4. Next, using the pantograph pulley free body

diagram, we quickly conclude that the two pantograph cable tensions between C_1 and B_4 are identical to the two t_C previously found (from $\Sigma M_z = 0$ for the pulley). Then, we use all three force components in the $\Sigma \boldsymbol{F} = 0$ vector equation to find the internal force of the boom acting on the pulley at the C_1 pin joint. Finally, the remaining unknowns t_{B1} and t_{B2} are found from the boom free body diagram and $\Sigma \boldsymbol{M} = 0$, in {2} coordinates. In this case, the x moment component yields $0 = 0$ and can be ignored; simultaneous solution of the linear equations resulting from the y and z moment components yields t_{B1} and t_{B2}. Now, this completes the outline of the statics solution for design purposes in this article; for completeness, one could use the $\Sigma \boldsymbol{F} = 0$ vector equation to find the internal force of the boom acting on the base at the universal joint located at B_0, for design of the universal joint.

The two pantograph cable tensions t_C are guaranteed to remain in tension, by the design of the pantograph portion of the system (except in the case of certain extreme dynamic motions down, which must be avoided); boom-moving cable tensions t_{B1} and t_{B2} can become slack under quasi-static conditions, discussed in the following subsection along with statics design plots.

3.4.3. Mast statics results

Out of the nine unknowns (three scalar tensions and three 2-component vector forces) solved in the previous subsection, we will now present actual tensions t_C and t_{B1} for our mast design. The internal joint forces can also be important for system design, in sizing the members to handle the stress. Furthermore, due to symmetry, actual tensions t_{B1} and t_{B2} have symmetric behavior with regard to θ_1. The statics results for our mast design are shown in Fig. 15.

We assumed that identical 1000 N weights act vertically down at each of the four points C_i, $i = 1,2,3,4$, for all motion. Real passive cable tensions t_C do not change much for either variations in θ_1 or θ_2; the magnitude generally stays below 1500 N. Active mast cable tension t_{B1} stays relatively constant (decreasing slightly), as θ_2 increases, for a given θ_1. Again, the partner tension t_{B2} is less than t_{B1} for positive θ_1, with a similar shape as t_{B1} in Fig. 15; for negative θ_1, t_{B2} is identical to the t_{B1} shown in Fig. 15. The magnitude of t_{B1} is generally much greater than that of t_C, at least an order of magnitude greater.

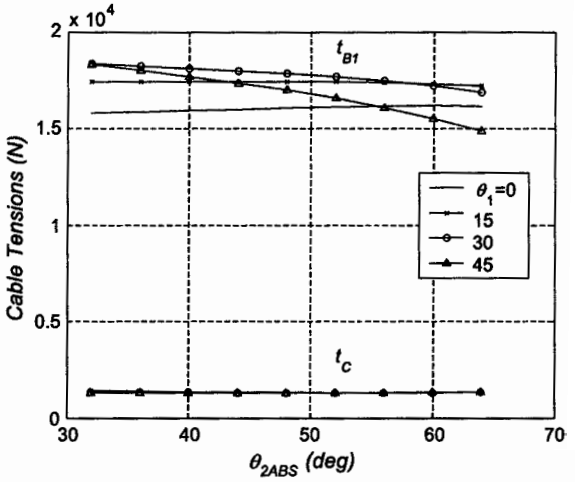

Fig. 15. Mast statics results.

This is due to a longer moment arm to the load for t_{B1} compared to that of t_C.

4. Alternate mobility system

Alternate designs are possible for our mobility system concept (see Fig. 4), depending on specific applications, workspace reach requirements, loads, and other considerations. In this section, we consider four aspects in Fig. 5 that can be modified: (1) the primary mast boom C_1B_0 can be rigid or telescoping; (2) there can be three heavy lift cables L_1, L_2, L_3, or a single heavy lift cable; (3) the pantographlike mechanism for attempting to maintain horizontal RoboCrane support points $C_2C_3C_4$ can be active or passive; and (4) we can use an equilateral triangle support $C_2C_3C_4$ as shown in Fig. 4, or a mast with cross spar and jib.

The design concept of Fig. 4 shows a rigid primary mast boom, three heavy lift cables, passive pantographlike mechanism, and equilateral triangle support. By contrast, Fig. 16 below shows a telescoping primary mast boom, a single heavy lift cable L_L, active pantographlike mechanism, and mast with cross spar and jib. These design features may be mixed and matched as desired to accomplish specific design goals for various construction applications.

In Fig. 16, the active pantographlike cable is controlled by a motor and winch at B_4; it passes over a pulley above point C_1 and connects to moving point

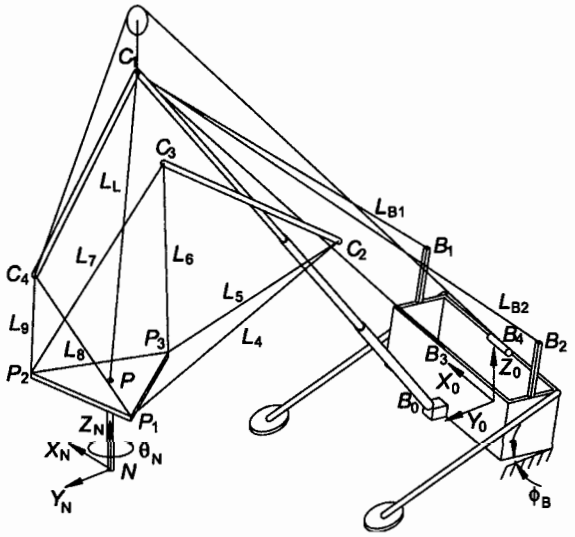

Fig. 16. Alternate NIST self-contained mobility system.

C_4. It is theoretically possible in this case to ensure that plane $C_2C_3C_4$ is always horizontal in the world frame. The jib is a rigid link C_1C_4 that is hinged via revolute joint at point C_1. The single heavy lift cable connects to the centroid P of the moving platform, runs over a pulley (not shown) at point C_1, and is actuated by a heavy lift motor at point B_3. The primary mast C_1B_0 telescopes; the end member $C_1C_2C_3$ is a rigid cross-shaped member.

For all designs, we can use the same base dumpster with tilting, the same mast-moving cables, and the same moving platform with turntable, plus nozzle or tools.

The role of the Fig. 16 mast is again to provide self-contained mobility for the RoboCrane-like portion of the automated construction mobility robot. Jib tip point C_4 is actively controlled by a variable cable length $L_{\text{jib}} = l_1 + l_2$, connecting C_4 to B_4 over a pulley, controlled to ensure that virtual isosceles triangle $C_2C_3C_4$ is horizontal for all motion.

5. Proposed controller concept

To satisfy commanded Cartesian trajectories, we propose the following controller. Given a series of commanded Cartesian poses, we use the inverse pose kinematics solution of Section 3.3 to calculate the required cable lengths (all mast and moving platform cables) at each control step. Each of these commanded cable lengths will be achieved at a high control update rate (say 1000 Hz) via the motors and cable reels, with joint encoders and a rotary-to-linear mapping for actual cable length feedback.

According to NIST RoboCrane hardware experience, cable length sensing using encoders in the load path does not yield sufficient accuracy for the construction task. Therefore, we also propose a Cartesian metrology system (a noncontact laser-based 6-*df* system independent of the robot) to provide an outer-loop controller that can run slower (say 100 Hz) in order to provide a servo to reduce errors in the Cartesian pose, due to real-world issues such as modeling uncertainties, cable stretch, wear, and flexibility, plus wind loads.

In future work, we will implement this controller, along with the equations of this article, in a Matlab/Simulink simulation, to determine a baseline controller design for real-world applications. We will also model cable flexibility and simulate real-world disturbances, such as wind loads, to test the robustness of the proposed controller. However, due to NIST hardware implementation and testing experience, we believe that our proposed controller with independent Cartesian metrology-based servo to task accuracy will be sufficient, even in nonlaboratory construction environments.

6. Conclusion

This article has presented two alternate design concepts for a novel automated construction system based on material deposition. We focus mainly on the self-contained, cable-suspended mobility system. The NIST RoboCrane has been developed as a stiff, stable crane device that controls all 6 degrees of freedom of the load. However, the standard RoboCrane requires rigid overhead support points for the six cables. This work is an attempt to extend the RoboCrane to a mobile, self-contained cable-suspended crane that provides its own rigid overhead cable support points.

We presented the overall system concept, and then derived kinematics equations for control of the cable-suspended mobility subsystem. We also considered statics analysis for the mobility system mast, and identified and calculated motion limits for avoiding

negative cable tensions during operation. We presented alternate mobility system concepts for the self-contained RoboCrane.

The Cartesian metrology system provides a means to achieve Cartesian trajectories in the face of uncertainties and unmodeled effects such as cable stretch, wear, and flexibility, plus wind loads. Industrial robots solve this problem by being bulky, stiff, and heavy, with large motors and low payload to weight ratios. Existing construction crane systems have stiff booms but also employ swinging cables that do not constrain all 6 degrees of freedom. The concept of this article provides a lightweight system with cable-suspended actuation that can provide stiffness in all 6 degrees of freedom. The metrology system will enable accurate control despite real-world uncertainties and disturbances.

Acknowledgements

The first author gratefully acknowledges support for this work from the NIST Intelligent Systems Division, via Grant #70NANB2H0130.

References

[1] J.S. Albus, R. Bostelman, N.G. Dagalakis, The NIST RoboCrane, Journal of Robotic Systems 10 (5) (1993) 709–724.

[2] J.S. Albus, Cable Arrangement and Lifting Platform for Stabilized Load Lifting. U.S. Patent 4,883,184 (November 28, 1989).

[3] T. Aria, H. Osumi, H. Yamaguchi, Assembly robot suspended by three wires with seven degrees of freedom, 11th International Conference on Assembly Automation, SME, Dearborn, MI, 1990, pp. MS90-807-1–MS90-807-13.5.

[4] R.V. Bostelman, J.S. Albus, A.M. Watt, Underwater Work Platform Support System. U.S. Patent 5,507,596 (April 16, 1996).

[5] J.J. Craig, Introduction to Robotics: Mechanics and Control, Addison-Wesley Publishing, Reading, MA, 1989.

[6] N.G. Dagalakis, J.S. Albus, B.-L. Wang, J. Unger, J.D. Lee, Stiffness study of a parallel link robot crane for shipbuilding applications, Journal of Offshore Mechanical and Architectural Engineering 111 (3) (1989) 183–193.

[7] B. Khoshnevis, Automated construction using contour crafting-applications on earth and beyond, 19th International Symposium on Automation and Robotics in Construction, Gaithersburg, MD, U.S. Government Printing Office, Washington D.C., 2002, pp. 489–494.

[8] M.M. Mikulas Jr., L.-F. Yang, Conceptual design of a multiple cable crane for planetary surface operations, NASA Technical Memorandum, vol. 104041, NASA LaRC, Hampton, VA, 1991.

[9] A.P. Shanmugasundram, F.C. Moon, Development of a parallel link crane: modeling and control of a system with unilateral cable constraints, ASME International Mechanical Engineering Congress and Exposition, San Francisco CA, DSC, vol. 57-1, 1995, pp. 55–65.

[10] W.-J. Shiang, D. Cannon, J. Gorman, Dynamic analysis of the cable array robotic crane, IEEE International Conference on Robotics and Automation, Detroit MI 4 (1999) 2495–2500.

[11] B.V. Viscomi, W.D. Michalerya, L.-W. Lu, Automated construction in the ATLSS integrated building systems, Automation in Construction 3 (1) (1994) 35–43.

[12] R.L. Williams II, J.S. Albus, R.V. Bostelman, Cable-based metrology system for sculpting assistance, ASME Design Technical Conferences, 29th Design Automation Conference, Chicago, IL, September 2-6.

[13] R.L. Williams II, P. Gallina, J. Vadia, Planar translational cable-direct-driven robots, Journal of Robotic Systems 20 (3) (2003) 107–120.

[14] M. Yamamoto, N. Yanai, A. Mohri, Inverse dynamics and control of crane-type manipulator, IEEE/RSJ International Conference on Intelligent Robots and Systems 2 (1999) 1228–1233.